Importance of proximal hydrogen bonds in haem proteins.

Jensen, Kasper; Ryde, Ulf

Published in:
Molecular Physics

DOI:
10.1080/0026897031000109383

2003

Document Version:
Peer reviewed version (aka post-print)

Importance of proximal hydrogen bonds in haem proteins

Kasper P. Jensen and Ulf Ryde

Department of Theoretical Chemistry

Lund University

Chemical Centre

P. O. Box 124

S-221 00 Lund

Sweden

Correspondence to Ulf Ryde

E-mail: Ulf.Ryde@teokem.lu.se

Tel: +46– 46– 2224502

Fax: +46– 46– 2224543

2017-04-09

We have used the density functional B3LYP method to study the effect of hydrogen bonds from the histidine ligand in various haem proteins to carboxyl groups or to the carbonyl backbone. Hydrogen bonds carbonyl groups (encountered in globins and cytochromes, for example) have a small influence on the geometry and properties of the haem site. However, hydrogen bonds to a carboxyl group (encountered in peroxidases and haem oxidase) may have a profound effect. The results indicate that in the Fe^{3+} state, this leads to a deprotonation of the histidine ligand, whereas in the Fe^{2+} state, the proton involved in the hydrogen bond may reside on either histidine or the carboxylate group, depending on the detailed structure of the surroundings. If the histidine is deprotonated, the axial Fe–N bond length decreases by 0.15 Å, whereas the equatorial bond lengths increase. Moreover, the charge on iron and histidine is reduced, as is the spin density on iron. Most importantly, the energy difference between the high-and intermediate-spin change so that whereas the two spin states are degenerate in the Fe^{2+} state for the protonated histidine, they are degenerate for the Fe^{+3} state when it is deprotonated. This may facilitate the spin-forbidden binding of dioxygen and peroxide substrates, which takes place for the Fe^{2+} state in globins but in the Fe^{3+} state in peroxidases. The reduction potential of the haem group decreases when it hydrogen-bonds to a negatively charged group. The inner-sphere reorganisation energy of the Fe^{2+} Fe^{3+} transition in a five-coordinate haem complex is ~30 kJ/mole, except when the histidine ligand is deprotonated without any hydrogen-bond interaction.

1. Introduction

Histidine (His) is probably the most common metal-binding ligand in biological systems [1]. The two nitrogen atoms of its imidazole ring can exhibit several protonation states depending on the chemical environment. The pK_a of His is ~14, whereas that of protonated His is 6–7 [2], so in aqueous solution, the amounts of neutral and protonated histidine are similar, with no deprotonated His available. However in proteins, and in particular under the influence of metals or other ionic groups, all modes of protonation of an imidazole ring are possible. An example is Cu,Zn superoxide dismutase, where an imidazolate group acts as a bridge between the two metals [1].

Both nitrogen atoms in the imidazole ring of His are excellent hydrogen-bond acceptors or donators, depending on the protonation state. When one of the nitrogen atoms coordinates to a metal ion, the other nitrogen atom becomes a strong hydrogen-bond donator through the polarisation effect of the metal ion; it has even been speculated that the imidazole ring may be deprotonated when it interacts with a negatively charged group, e.g. an aspartate or glutamate residue [3]. Of course, this would change the properties of the His ligand.

In haem proteins, His ligation is often encountered. The His ligand coordinates to the iron ion with one nitrogen atom, while the other nitrogen atom is free to form a hydrogen bond to adjacent hydrogen-bond acceptors. The proximal triad Fe–His–Asp/Glu is conserved in several haem proteins, including haem peroxidases (e.g. horseradish peroxidase [4]) and oxygenases (e.g. haem oxygenase [5,6]). The acidic residue has been assigned an important role for these enzymes [7], and this is one case for which it has been suggested that the His ligand might be deprotonated [3,8]. In other haem proteins, there is no acidic residue close to the His ligand and it then typically forms a hydrogen bond to a carbonyl group of the protein backbone (e.g. globins [9,10], cytochromes [11], cyclooxygenase [12], and cytochrome *c* oxidase [13]).

The role of second-sphere interactions and hydrogen-bond networks has attracted much interest within the field of haem proteins [3, 14-17]. In particular, it has been suggested that the negatively charged Cys or Tyr ligand in cytochrome P450 and catalases and the His ligand, hydrogen bonded to Asp, in peroxidase donates electron density to the iron ion, thereby promoting the cleavage of the O–O bond. This is the 'push' part of the well-known push–pull mechanism [7, 18]. Together with mutagenesis experiments, this suggest that proximal second-sphere interactions are important for catalytic activity of several His-ligated haem proteins [19].

It has been argued that metal sites buried in a low-dielectric protein must have

a net charge close to neutral, because of the strong Coulomb forces between to two charged centres [20, 21]. This, together with the fact that both ferric, ferrous, and sometimes high-valent oxidation states are important in haem chemistry, suggests that the protein could keep the charge of the active site low by a deprotonation–protonation equilibrium of imidazole. In particular, the ligand dyad Asp-His has been suggested to stabilise the Fe^{IV}=O (compound I/II) intermediates in peroxidase [3, 8, 22, 23]. A fully deprotonated His provides an extreme case in this regard, with strongly hydrogen–bonded His falling in the range between deprotonated and neutral His, as has been evidenced by structural and magnetic data [24]. Indeed, it has been pointed out [25] that 'the effect of hydrogen bonding on the donor group is in the same direction as the effect of ionisation, but less extreme'.

Haem iron may exist in low-, intermediate-, or high-spin states, depending on the nature of the axial ligands. In many haem enzymes, the spin state of the intermediates are important for the catalytic mechanism [26, 27]. It is conceivable that the His ligand of peroxidases can affect the relative stability of spin states by tuning the axial ligand-field strength. The hydrogen-bond interaction may also affect the location of the organic radicals present during peroxidase activity, as has been discussed for cytochrome *c* peroxidase and ascorbate peroxidase [28].

A special case where tuning of the axial ligand strength may be important is electron transfer. According to Marcus theory, the rate of electron transfer can be described by an Eyring equation,

$$k = A \exp(- \qquad G$$

where A is a preexponential factor that depends on the coupling between wave functions before and after electron transfer and G is the activation free energy of the reaction. The latter is expressed as a function of the reduction potential, G , and reorganisation energy of electron transfer, :

$$G \qquad\qquad G^{0}/)^{2} \qquad (2)$$

The reorganisation energy measures how much energy is needed to change the structure during the redox reaction [29]. It is conceivable that hydrogen bonds may reduce the change in geometry of haem during electron transfer, thereby reducing the reorganisation energy.

Second-sphere interactions also have a strong influence on the reduction potentials. For example, mutagenesis studies of the haem ligand and its environment

in peroxidases have shown that the $Fe^{+2/+3}$ potential decreases as the negative charge of the haem ligand increases [30, 31]. A similar effect has been suggested for catalases and cytochrome P450 [32].

Recently, several theoretical studies of second-sphere interactions in haem proteins have been presented. For, example, the effect of hydrogen bonds on vibrational frequencies in carbon monoxy iron porphine has been investigated [33], as well as the localisation of the radical site in cytochrome *c* peroxidase and ascorbate peroxidase [34]. A third study tried to understand compound I formation in haem peroxidases by including models of Asp and Trp as proximal second-sphere ligands [35]. Other theoretical studies have considered how the first-sphere imidazolate ligand may affect the electronic structure and spin coupling constants of the compound I/II models of peroxidases [36-38].

In the present paper, we use similar theoretical methods to address the importance of hydrogen bonds to carbonyl and acidic groups for a His-ligated haem group. We investigate in detail how the electronic structure changes in a series of biologically relevant hydrogen-bond networks. In particular, we study the nature of these networks and the structures, energetics, reduction potentials, reorganisation energies, and other properties of the haem cofactor.

2. Methods

2.1 Computational details

All calculations were performed with the density functional Becke three-parameter hybrid method with the local spin-density approximation correlation functional of Vosko–Wilk–Nusair and the non-local Lee–Yang–Parr correlation functional (B3LYP) [21,39-44]. B3LYP is widely recognised as one of the most accurate density functional methods, in general terms, for structures, energies, and frequencies [45,46]. It has been shown to give excellent geometries for transition metal complexes with errors in the metal bond distances of 0–5 pm [47-50] and mean absolute errors in energies of less than 20 kJ/mole [21,47].

The calculations were carried out with the Turbomole software, version 5.3 [51]. The basis sets used for geometry optimisation were 6-31G(d) for all atoms except iron. This basis set assigns one set of polarisation functions to all non-hydrogen atoms. Iron was described by the double- basis set of Schäfer *et al.* [49], augmented with two *p*, one *d*, and one *f* functions [52] with the contraction scheme (14s11p6d1f) / [8s7p4d1f]. Only the pure five *d* and seven *f*-type functions were used.

We applied the default (m3) grid size of Turbomole, and all optimisations were carried out in redundant internal coordinates. Unrestricted calculations were

performed for the open-shell systems. We made use of default convergence criteria, which imply self-consistency down to 10^{-6} Hartree (2.6 J/mole) for the energy and 10^{-3} a.u. (0.053 pm or 0.057°) for the internal coordinates. The largest calculations innvolved 1240 basis functions.

2.2 Solvation energies and reduction potentials

Standard quantum chemical calculations are performed in vacuum (gas phase), whereas biological reactions take place in water solution or in proteins. In order to correct for this discrepancy, we have calculated solvation energies for most complexes using the continuum conductor-like screening model (COSMO) model [53], as implemented in Turbomole 5.5. In this method, the solute molecule forms a cavity within a dielectric continuum characterised by a dielectric constant, . The charge distribution of the solute polarises the dielectric medium and the response of the medium is described by screening charges on the surface of the cavity.

These calculations were performed with default values for all parameters (implying a water-like probe molecule) and with a dielectric constant of 4 and 80, to model pure water and to get a feeling of possible effects in a protein (where the effective dielectric constant is normally estimated to be 2–16) [54-55]. For the generation of the cavity, a set of atomic radii has to be defined. We used the optimised COSMO radii in Turbomole (H: 1.30 Å, C: 2.00 Å, N: 1.83 Å, O: 1.72 Å, Fe: 2.00 Å).

Reduction potentials were estimated from these energies in a solvent according to:

$$E^0 = E(\text{ox}) - E(\text{red}) - 4.43 \qquad (3)$$

where the term 4.43 eV represents the potential of the standard hydrogen electrode [56].

2.3 Model systems

All the investigated models are five-coordinate deoxyhaem structures, which include the porphine unit without any side chains. This is the fundamental geometrical unit of porphyrin modelling, since smaller models destroy the conjugation of the porphyrin ring, whereas larger models are computationally expensive and have insignificant effect on the haem electronic structure [57]. As the proximal axial ligand, we have applied imidazole (Im) and imidazolate. In addition, $Im(CH_2)_2CHO$, Im + CH_3COO^- and $Im(CH_2)_2CHO$ + CH_3COO^- have been studied as models of various possible second-sphere environments.

The five investigated models are shown in Figure 1. For all models, the geometries of both the Fe^{II} and Fe^{III} systems were optimised in the three possible spin states. Model **1**, which includes the porphine ring and a neutral imidazole, represents the haem prosthetic group with only the proximal His. This model has no second-sphere interactions at all and has been the standard model in theoretical studies of deoxyhaem systems [58-61]. Model **2** is identical to **1** except that the imidazole has been deprotonated to yield a negatively charged imidazolate ligand. This model serves as a limiting case, where the proton has been completely transferred to its hydrogen-bond partner. The three models **3**–**5** are realistic intermediate models of haem with various types of hydrogen-bond interactions. In model **3**, we included the and carbons, as well as the carbonyl group of the His peptide backbone. This was done to test the properties of a weak hydrogen bond from a carbonyl group. Such a hydrogen bond is present in many haem proteins, including globins and cytochromes [8–10]. Model **4** represents haem where the His ligand hydrogen bonds to an adjacent acetate group, which is a model of either Asp or Glu. This situation is encountered in haem peroxidases. Finally, model **5** is the largest model and includes both the backbone carbonyl and the acetate group. The two groups compete for the imidazole proton together with imidazole. Such a situation is found in haem oxygenase [62]. All optimisations of models **3**–**5** started with a neutral imidazole group. To evaluate the energies of the hydrogen bond minima, we also constrained the proton–acceptor distances to certain values and relaxed all other degrees of freedom. These relaxed scans also provide information about the change in chemical properties of the haem site when the proton is exchanged between the two groups.

3. Results and Discussion

3.1 Geometries of the optimised models

In Table 1, the optimised Fe–N bond distances are presented for the three possible spin states of the five models. Model **1** was constructed to mimic a five-coordinate haem group with only a proximal His ligand. This model has been studied theoretically by several groups before [58-61] and we only use it as a reference when comparing with the other models.

In model **2**, the imidazole ligand in model **1** has been deprotonated to imidazolate. This complex constitutes the extreme case where the proton has been completely transferred to its hydrogen-bond acceptor, and will be used as a reference for that situation. This model has also been studied in earlier calculations [63] and we only note that the most prominent effect of deprotonating the iron ligand is that the $Fe–N_{Im}$ bond shortens by 0.15–0.22 Å, whereas the equatorial bonds increase by 0.01–

0.06 Å. At the same time, the distance of the iron ion out of the haem plane increases, especially in the high-spin state (by 0.11–0.34 Å).

An interesting observation, which holds true for both models **1** and **2**, is that although low-spin (LS) state always has the shortest bonds (both axial and equatorial), the axial bond is longer in the intermediate spin (IS) state than in the high-spin (HS) state, whereas the equatorial bonds are longer in the HS than in the IS state. This is an effect of the orbital occupations. The IS system has one electron in the d_{z^2} orbital, which is directed towards the axial ligand. Therefore, the axial bond is long in the IS state. However, the HS system has also one electron in the $d_{x^2-y^2}$ orbital, which is directed towards the equatorial ligands. This means that both axial and equatorial bonds are elongated by increased electron repulsion. The elongation of the bonds to the equatorial ligands reduces the ligand–ligand repulsion and therefore makes the axial bond relatively short.

The case of a weak hydrogen bond to a carbonyl group is evaluated by model **3**. As expected, the proton remains on imidazole in this interaction and therefore, the geometry of this model closely resembles that of model **1** to within 0.002 Å for equatorial bond lengths and 0.03 Å for the more flexible axial bond lengths. The hydrogen bond distances are very similar in the ferrous and ferric states (2.07–2.09 Å for O–H and 1.01–1.02 Å for N–H). Apparently, the hydrogen bond in model **3** does not affect the structure of the haem system, and therefore, such an interaction will probably not affect the function of the haem protein significantly.

In some enzymes, in particular the haem peroxidases, the His ligand forms a hydrogen bond to an Asp or Glu residue. We describe this situation by model **4**, where acidic residue is modelled by an acetate group. All optimisations were started with the hydrogen atom involved in the hydrogen bond on imidazole. However, during the geometry optimisation, the hydrogen atom moved to the acetate ion in all ferric systems and also in the ferrous LS state. Thus, the effect of the hydrogen bond is not only an electrostatic perturbation of the ligand field, but it may rather affect the protonation state of the ligand and thereby drastically change the ligand field.

For the biologically relevant HS states, we investigated thoroughly the energy difference between the two hydrogen-bond types (NH–O or N–HO). For the ferrous complexes, both types could be optimised, with the NH–O type being most stable by 1 kJ/mole in vacuum. For the ferric model, no local minimum was found for the NH–O bond type. An energy difference of 37 kJ/mole between the two types of hydrogen bonds was obtained if the N–H bond length was fixed to 1.11 Å.

It is conceivable that this transfer of the hydrogen atom is a pure vacuum effect. Therefore, the calculations were repeated in water solution. However, this did

not change the preference, as can be seen in Table 2. For the ferrous model, the difference between the two hydrogen-bond types has increased to 10 kJ/mole. For the ferric model, a local minimum of the NH–O type is obtained if the geometry is optimised in solution at dielectric constants 8. Interestingly, in aqueous solution the energy difference is only 4 kJ/mole.

From the equilibrium distances in Table 1, it can be seen that model **4** looks essentially like the imidazolate model **2**, within 0.02 Å in the Fe–N distances, when the proton resides on acetate. However, when the proton resides on imidazole, the structure is similar to that of model **1**, but the flexible Fe–N_{Im} bond length has decreased by 0.10–0.13 Å and the equatorial distances have increased by 0.01–0.04 Å. This is of course an effect of the increased electron density on the imidazole ligand caused by the hydrogen bond to the acetate ion.

For the HS ferrous model, we have also studied the energy profile of the transfer of the proton from imidazole to acetate. The results in Figure 2 illustrate the flexibility of the hydrogen position. From the topology of the energy profile, a barrier for proton transfer in vacuum of ~3 kJ/mole can be estimated. In water solution, the barrier increases to ~11 kJ/mole. This corresponds to a rate of proton transfer of ~10^8 s^{-1}, i.e. close to the diffusion limit.

The flexibility of the potential surface in Figure 2 indicates that displacement of the N–H bond of the peroxidase model **4** may be achieved very easily. Therefore, we have studied how such fluctuations may change the structure and electronic properties of the model. The results in Figure 3 show that the charge on iron is insensitive to variations in the N–H distance, whereas the fluctuation in the Fe–N_{Im} distance is substantial (a variation of 0.07 and 0.02 Å for the ferric and ferrous states, respectively, when the N–H bond length is varied by 0.35 Å). Interestingly, all of the change in the Fe–N_{Im} distance can be attributed to the change in the distance of the iron ion out of the porphyrin plane. This shows that the proximal hydrogen bond has a direct effect on the geometry of the haem complex. Similar fluctuations have been reported in a recent spectroscopic study [64].

The largest model **5** describes the situation where both a carbonyl group and an acidic hydrogen-bond acceptor are present at the same time to compete for the proton at imidazole. This situation resembles that of human haem oxygenase-I [62].

It turns out that the structural effect of including the His backbone and carbonyl group is negligible. As can be seen in Figure 1e, the carbonyl group does not interact with the imidazole ring in our vacuum structure. Instead, it forms a weak hydrogen bond to the methyl group of acetate. Yet, steric interactions between the backbone and the acetate group change the binding mode of the latter group from *syn*

to *anti* (the acetate group binds with the lone electron pair close to the carbon atom and not that close to the other carboxyl oxygen) [1]. Such a binding mode is also encountered in haem oxygenase [62]. In general, the *anti* lone-pair is less basic and forms slightly weaker hydrogen bonds [65]. Therefore, it is interesting to study also such an interaction. Moreover, the inclusion of the backbone gives a more realistic model of His.

The optimised geometric parameters of model **5** are collected in Table 1. They are quite similar to those obtained for model **4**. In particular, the hydrogen atom moves to acetate for all ferric complexes and for the HS ferrous complex. Interestingly, for this model, it was possible to optimise the two hydrogen-bond types (NH–O and N–HO) in both the ferric and ferrous HS states. As can be seen in Table 2, the NH–O tautomer is the more stable in both oxidation states, but the energy difference is not very large, 10 kJ/mole for the ferric state and 1 kJ/mole for the ferrous state. In water solution, the difference changes by 2–3 kJ/mole. The stabilisation of the N–HO tautomer is probably an effect of the *anti* hydrogen bond in this complex.

Figures 4 and 5 show the energy profiles of the hydrogen bond for the ferric and ferrous HS states in vacuum and solution, respectively. As for model **4**, the ferrous energy surfaces are very flexible with a small barrier.

3.2 Energy order of spin states

Table 3 shows the relative energies of the various spin states for ferrous and ferric haem models **1**–**5**. For the ferric models **1** and **3**, IS is preferred by 21–24 kJ/mole over HS, whereas LS is 42–48 kJ/mole less stable. For the ferrous models **1** and **3**, IS is also most stable, but only by 3–4 kJ/mole compared to HS, so this difference is within the uncertainty of the method, and indicates a possibility of spin crossover. Since the results of model **3** resemble those of model **1** so closely, we can conclude that the carbonyl group does not affect the ligand field.

Solvation has only a small effect (1–6 kJ/mole) on the order of the spin states, but it favours the HS state and makes the HS and IS states almost degenerate for ferrous **1** and **3**. The results for model **1** are similar to what have been found in earlier studies [60, 61]. However, they are at variance with the experimental observation that five-coordinate haem complexes are HS both in proteins and in model systems [26]. This reflects that it is much harder to estimate the energy difference between states with different multiplicity than with same multiplicity, because of their differing exchange-correlation energies. Therefore, the accuracy of the energies in Table 3 is lower than the other energies presented in this work.

The imidazolate model **2** has a HS ground state for both the ferrous and ferric forms, but for the latter, the energy gap to the IS is small (7 kJ/mole), and solvation renders IS the ground state. In the ferric form, both models **4** and **5** are similar to model **2**, as could be expected from their N–HO type of hydrogen bond, even if the ferric form of model **5** has an IS state slightly more stable than the HS state. For the ferrous complexes, the comparison is complicated by the fact that the optimum structures of the various spin states of model **4** and **5** have different types of hydrogen bonds. However, both models have HS ground states.

The present results are not reliable enough to draw any firm quantitative conclusions, but the trends allow us to divide the models into two groups, with model **3** resembling neutral deoxyhaem **1**, and models **4** and **5** resembling haem with deprotonated imidazole **2**. The qualitative difference in the order of spin states shows directly that the hydrogen-bond frameworks, by means of controlling the basicity of imidazole, can tune the splitting energies by affecting the axial ligand field of the metal site.

The main difference between the imidazole- and imidazolate-like structures is that in the former, the HS and IS ferrous states have similar energies, whereas for the latter it is the ferric states that are close to spin crossover. This is in accordance with resonance Raman spectra of horseradish peroxidase [66] and barley peroxidase [67] systems, which revealed a quantum admixed ferric S = 3/2, 5/2 five-coordinate species. The same studies suggested that the quantum-admixed state is common to a whole class of peroxidases.

It then seems tempting to suggest that the hydrogen bond to an acidic residue in peroxidases and the absence of such a bond in haemoglobin, cyclooxygenase-I, and cytochrome *c* oxidase, may be a means to facilitate the binding of the oxygen-containing substrate, which is spin-forbidden in the high-spin state (the six-coordinate binding product is LS). The peroxidases bind peroxide to the Fe^{3+} state, whereas the other three proteins bind O_2 to the Fe^{2+} state, in accordance with the state predicted to be close to spin crossover.

3.3 Electronic structure

In Table 4, we have collected the results of Mulliken population analysis of the investigated complexes. We list the charges of iron q(Fe), the axial nitrogen atom $q(N_{Im})$, the average atomic charge of the four equatorial nitrogens $q(N_{eq})_{av}$, together with the spin densities on iron, N_{eq}, and N_{Im}. This table provides a picture of the charge and spin distribution in the ligand field, and how it changes with oxidation

state, spin state, and the presence of a hydrogen bond.

If we look at the charges first, an important observation is that the charge distribution in ferric complexes is barely affected by the proximal environment: The charge on ferric iron is always 0.99–1.01 for HS, 0.87–0.89 for IS, and 0.79–0.82 for LS. The charges on the equatorial nitrogens are similar as well, whereas the charge on the axial nitrogen is 0.01–0.07 more negative in models **2**, **4**, and **5**, in which the imidazole ligand is more electron-rich. For the ferrous HS complexes, the charge on both iron and axial nitrogen is ~0.1 more negative in models **2** , **4**, and **5** than in models **1** and **3**. This shows that the electronic structure of **4** is similar to that of **2**, effectively increasing the electron density at iron and axial nitrogen by 0.2 together. This correlates with the shorter axial bond lengths of these complexes (Table 1). Hence, the ability of a hydrogen bonded structure to donate more electrons to the iron centre, both relevant for a push effect and for stabilisation of high oxidation states, is witnessed in the calculations.

The spin densities describe where in space the and densities do not cancel. The spin densities obtained at iron with Mulliken population analysis are usually somewhat smaller than expected from the formal spin state iron. This is because the spin is delocalised into the ligands. For all ferric HS models, the iron spin density is 4.16–4.19, with additional 0.45–0.51 spin delocalised into the equatorial nitrogen atoms and 0.09–0.20 delocalised into the axial nitrogen. The effect of hydrogen bonding is clearly seen in the HS models: The models **2**, **4**, and **5** have 0.07–0.11 more spin density on N_{Im}, ~0.06 less spin density on N_{eq}, and 0.01–0.03 less spin density on the iron ion.

Likewise, the HS ferrous models **2** , **4**, and **5** have 0.08 less spin density on iron than models **1** and **3**, delocalised into other regions of the molecules. Interestingly, the electronic structure of the NH–O tautomer of ferrous model **4** is similar to the N–HO (and therefore to model **2**), whereas the same tautomer of model **5** is most similar to model **1**. The correlation between hydrogen bonds and spin density indicates that the electronic structure on iron is changed significantly by the hydrogen bonds.

3.4 Reorganisation energies

The cytochromes are well-known electron carriers in biological systems. They contain six-coordinate haem groups with two axial ligands, normally at least one His

residue. These sites exhibit very small inner-sphere reorganisation energies (~8 kJ/mole [49]) and therefore seem to be ideal electron-transfer sites. However, the reaction mechanism of many other haem enzymes involves steps of electron transfer even in the five-coordinate state, e.g. cytochrome P450 and haem oxygenase [6]. Therefore, it may be interesting to see how the reorganisation energy of our five-coordinate haem models varies as a function of the hydrogen-bond pattern to the His ligand.

We have calculated the self-exchange inner-sphere reorganisation energies of all five models, as the energy difference between the optimum Fe^{2+} structure and the optimum Fe^{3+} structure, calculated with either an oxidised (Fe^{3+}) wavefunction ($_{ox}$) or a reduced (Fe^{2+}) wavefunction ($_{red}$):

$$_{red} \quad E(Fe^{II} \text{ with } Fe^{III} \text{ structure}) - E(Fe^{II} \text{ with } Fe^{II} \text{ structure})$$

$$_{ox} \quad E(Fe^{III} \text{ with } Fe^{II} \text{ structure}) - E(Fe^{III} \text{ with } Fe^{III} \text{ structure})$$

$$= _{red} + _{ox}$$

The results of these calculations are collected in Table 5. All reorganisation energies of these five-coordinate are rather high (48–97 kJ/mole), compared to six-coordinate models of cytochromes with various sets of axial ligands (4–8 kJ/mole) [49]. There are three important reasons for this: For model **1**, with a neutral imidazole ligand, the increased reorganisation energy (28 kJ/mole) comes from the larger difference in the bond length of both the axial and equatorial ligands (0.11 and 0.02 Å, compared to 0.03 and 0.01 Å for the corresponding six-coordinate model with two imidazole ligands [49]). For model **2**, the even larger reorganisation energy (61 kJ/mole) comes from the change to a negatively charged axial ligand, which gives stiffer bonds. Thus, even if the change in the Fe–N_{Im} bond length is smaller (0.09 Å) than in model **1**, this gives rise to a larger energy term (in combination with the increased change in the equatorial bond lengths, 0.06 Å). A similar effect was observed for six-coordinate models with a negatively charged Cys, Tyr, or Glu ligand (= 20–47 kJ/mole) [49].

Finally, for the hydrogen-bonded models **3**–**5**, the increase in the reorganisation energy may also arise from the acetate group and from the carbonyl backbone, which make the systems larger and include some components of the outer-sphere reorganisation energy. To avoid these components, which make the results harder to interpret, we have also calculated the reorganisation energy of models **3**–**5**, after cutting off these parts (i.e. the reorganisation energy is calculated only for the atoms in model **1** or **2**, depending of the hydrogen-bond type) but without any change

of the geometry. These results are also included in Table 5 and give smaller and more similar results (29–33 kJ/mole), as expected. It may at first seem somewhat unexpected that the reorganisation energies of models **4** and **5** are so much lower than for model **2**, but the reason for this seems to be the smaller change in the bond lengths to the equatorial ligands (0.02–0.05 Å), partly compensated for by an increased change in the axial bond length (0.10–0.14 Å).

Thus, we can conclude that a deprotonation of the imidazole ligand would increase the reorganisation energy, but the hydrogen-bond networks encountered in proteins compensate fully for this effect, so that the reorganisation energy does not increase at all, independent of the position of the hydrogen atom.

Even if the calculated reorganisation energy of these five-coordinate complexes is appreciably higher than what has been observed for six-coordinate cytochrome models, such a reorganisation energy (~30 kJ/mole) is not prohibitively high for electron transfer. On the contrary, similar reorganisation energies have been calculated for the other two groups of electron carriers in nature, blue copper proteins and iron–sulphur clusters (20–44 kJ/mole) [68,69]. Moreover, it must be remembered that the outer-sphere contribution is also important for the reorganisation energy and that there are more terms in the Marcus equation (Eqns. 1–2) that may compensate for a relatively high reorganisation energy, e.g. the reduction potential.

3.5 Reduction potentials

The reduction potential of a haem site is sensitive to the nature of the axial ligands and to the environment around the site, as has been shown by site-directed mutagenesis [31]. Therefore, it could be interesting to study how the reduction potentials change in our model systems. The reduction potentials were calculated according to Eqn. (3) at dielectric constants of 1, 4, and 80, and the results are collected in Table 6.

Models **1** and **2** show the limiting behaviours: Model **1** has a quite high potential –0.34 V in aqueous solution and 0.03 V at = 4. Model **2**, on the other hand, has a lower potential, –0.66 V in aqueous solution and –1.21 at = 4. Thus, the potential of model **1** decreases when the dielectric constant is increased, whereas that of model **2** increases. This is of course an effect of the total charge of the complexes. For model **1**, the reduced form is neutral and the oxidised form has a charge of +1, whereas for model **2**, the reduced form has a charge of –1, whereas the oxidised form is neutral. Solvation will always favour the charged species (the Born solvation energy is proportional to the charge squared), so it will decrease the reduction potential of model **1** and increase it for model **2**, exactly as observed.

Models **3**–**5** exhibit an intermediate behaviour. Model **3** has the same charge as model **1** and its potentials are also similar to those of this model, but the hydrogen bond to the carbonyl group makes them slightly more negative (by 0.03–0.14 V). Models **4** and **5** have the same total charge as model **2** and therefore the potentials increase when the dielectric constant is increased. However, for these systems, the potential depends quite strongly on whether the hydrogen atom resides on acetate or imidazole. In general, the potentials of model **4**, with its strong interaction between acetate and imidazole, are quite close to those of model **2**, whereas those of model **5**, with its weaker *anti* interaction, are intermediate between model **1** and **2**, at least in aqueous solution (–0.50 to –0.39 V). Thus, the reduction potential is a sensitive probe of the electrostatic environment in the haem site.

The effective dielectric constant in proteins is normally estimated to be in the range 2–16 [54, 55]. Therefore, our calculated reduction potentials at = 1, 4, and 80 should embrace experimentally observed potentials. The observed reduction potential of five-coordinate myoglobin is 0.05 V and that of cytochrome *c* oxidase is 0.4 V [1]. This is within the range calculated for models **1** and **3**, 0.86 to –0.34 V, and most similar to the values obtained at low dielectric constants. However, the reduction potential of horseradish peroxidase, –0.22 V [1, 70], is slightly outside the range calculated for models 2, 4, and 5 (–2.31 to –0.39 V), which is not unexpected for these crude models. Yet, our calculations nicely reproduce the shift to negative potentials of the potential for peroxidase, as well as the experimental observation that the potential decreases as the negative charge of the haem ligand increases.

3.6 Concluding remarks

In this paper we have studied how the geometric, electronic, and functional properties of five-coordinate haem models are modulated by hydrogen bonds to the imidazole ligand. The fact that all peroxidases exhibit a hydrogen bond to Asp, that haem oxidases have a hydrogen bond to Glu, whereas most other types of proteins only have hydrogen bonds to carbonyl groups strongly indicates that this network plays an important role in the function of the haem group.

The most important implication of our results is that hydrogen bonds to acidic residues probably leads to deprotonation of the imidazole ligand to imidazolate, at least for the oxidised Fe^{3+} state. The results in Table 2 show that for the oxidised model **4**, the hydrogen atom resides on the acetate model; we could not even find a local minimum with the proton on the imidazole ligand in vacuum. In a solvent with a reasonably high dielectric constant (8) the NH–O form also becomes a local

minimum and in water solution the energy difference is predicted to be only 4 kJ/mole. Therefore, it is likely that the oxidised state of peroxidases, which shows the same type of hydrogen bond and geometry as model **4**, has a deprotonated imidazolate haem ligand unless the local environment is very polar. This has a strong bearing for all theoretical and mechanistic studies of these enzymes.

For the reduced Fe^{2+} state, the results are much less clear. The result in Table 2 shows that the NH–O and N–HO hydrogen-bond types have a similar energy, which also depends on the effective dielectric constant of the environment. Therefore, we cannot decide from the present results whether the reduced state of peroxidases has an imidazolate or imidazole ligand. This depends strongly on the detailed structure of the surroundings of the active haem site. A similar situation has been observed for compound 1 in peroxidases and for the catalytic zinc site in alcohol dehydrogenase ($Zn^{2+}Cys_2His$ Asp) [36, 71].

For haem oxygenase, which has a geometry more similar to model **5**, with the acetate group binding in an *anti* configuration, the situation is even more complicated: The reduced form has the same degeneracy as the peroxidase model, but for the oxidised state there exist a local minimum for the form with the proton on imidazole and the energy difference is not very large, 7–10 kJ/mole. Therefore, we cannot decide the position of the hydrogen atom in any oxidation state in haem oxygenase.

Furthermore, the actual position of the hydrogen atom is important. We have seen that for most properties studied the hydrogen bond has a discrete rather than continuous effect, i.e. that depending on whether the hydrogen atom resides on imidazole or acetate, the system is similar either to the imidazole model **1** or to the imidazolate model **2**. Only the reduction potential at high dielectric constant shows an almost continuous change depending on the strength of the hydrogen bond.

We have seen that the imidazolate complex has a 0.15 Å shorter $Fe–N_{Im}$ bond and 0.03–0.06 Å longer $Fe–N_{eq}$ bond lengths. Moreover, the imidazolate complexes have a lower charge on the iron and N_{Im} atoms, as well as a lower spin density on iron. However, the differences were not very large, so the functional significance of these differences are not clear. It is these small differences that would give rise to the much discussed push part of the push–pull effect and also to a differential stabilisation of high oxidation states of iron, e.g. the Fe^{IV} state of compound I in haem peroxidases. Further mechanistic investigations are necessary to study such effects in a more conclusive manner.

The most prominent features of the imidazole and imidazolate complexes seem to be the energy difference between the HS and IS complexes. For imidazole complexes, the reduced states seem to be almost degenerate, whereas for the

imidazolate complexes, it is rather the oxidised complexes that are degenerate. As discussed above, this may be used by the enzymes to facilitate the binding of the appropriate ligand (dioxygen or peroxide) at the right oxidation state.

Finally, we have seen that any type of hydrogen bond reduces the reorganisation energy for the imidazolate complex to a value similar to that of the imidazole model, ~30 kJ/mole. Thus, we can conclude that hydrogen bonds between the His ligand and various groups in haem proteins have a large and important effect on the both the structure and functional properties of the haem group.

Acknowledgements. This investigation has been supported by grants from the Swedish research council (VR) and by computer resources of d Lunarc at Lund University.

4. References

[1] Kaim, W., and Schwederski, B., 1994, *Bioinorganic chemistry: Inorganic elements in the chemistry of life. An introduction and guide*, John Wiley & Sons, Chichester, p. 18.
[2] Holm, R. H., Kennepohl, P. and Solomon, E. I. 1996, Chem. Rev. 96, 2239-2314.
[3] Valentine, J. S., Sheridan, R. P., Allen, L. C., and Kahn, P. C., 1979, *Proc. Natl. Acad. Sci. USA*, **76**, 1009.
[4] Henriksen, A., Schuller, D. J., Meno, K., Smith, A. T., Welinder, K. G., and Gajhede, M., 1998, *Biochemistry*, **37**, 8054.
[5] Schuller, D. J., Wilks, A., Ortiz de Montellano, P. R., and Poulos, T. L., 1998, *Protein Sci.*, **7**, 1836.
[6] Sono, M., Roach, M. P., Coulter, E. D., and Dawson, J. H., 1996, *Chem. Rev.*, **96**, 2841.
[7] Dawson, J. H., 1988, *Science*, **240**, 433.
[8] Finzel, B. C., Poulos, T. L., and Kraut, J., 1984, *J. Biol. Chem*., **259**, 13027.
[9] Silva, M. M., Rogers, P. H., and Arnone, A., 1992, *J. Biol. Chem.*, **267**, 17248. Pdb code: 1BBB.
[10] Tame, J., and Vallone, B. Pdb code: 1A3N.
[11] Matias, P. M., Coelho, R., Pereira, I. A., Coelho, A. V., Thompson, A. W., Sieker, L. C., Gall, J. L., and Carrondo, M. A., 1999, *Structure (London)*, **7**, 119.
[12] Picot, D., Loll, P. J., and Garavito, R. M., 1994, *Nature*, **367**, 243. Pdb code: 1PRH.
[13] Ostermeier, C., Harrenga, A., Ermler, U., and Michel, H., 1997, *Proc. Natl. Acad. Sci. USA*, **94**, 10547. Pdb code: 1AR1.
[14] Blumberg, W.E., and Peisach, J., 1971, *Adv. Chem. Ser.*, **100**, 271.
[15] Peisach, J., 1975, *Ann. N.Y. Acad. Sci*., **244**, 187.
[16] Morrison, M., and Schonbaum, R., 1976, *Annu. Rev. Biochem*., **45**, 861.
[17] Quinn, R., Nappa, M., and Valentine, J. S., 1982, *J. Am. Chem. Soc.*, **104**, 2588.
[18] Poulos, T. L., 1988, *Adv. Inorg. Biochem.*, **7**, 1.
[19] Newmyer, S. L., Sun, J., Loehr, T. M., and Ortiz de Montellano, P. R., 1996, *Biochemistry*, **35**, 12788.

[20] Lippard, S. J., Berg, J. M. *Principles of bioinorganic chemistry*, University science books, Mill Valley, CA, **1994**.
[21] Siegbahn, P. E. M., and Blomberg, M. R. A., 2000, *Chem. Rev.*, **100**, 421.
[22] Reed, C. A., Mashiko, T., Bentley, S. P., Kastner, M. E., Sheidt, R. W., Spartalian, K., and Lang, G., 1979, *J. Am. Chem. Soc.*, **101**, 2948.
[23] Goodin, D. B., 1996, *J. Biol. Inorg. Chem.*, **1**, 360.
[24] Landrum, J. T., Hatano, K., Sheidt, W. R., and Reed, C. A., 1980, *J. Am. Chem. Soc.*, **102**, 6729.
[25] Orgel, L. E., 1959, *Rev. Mod. Phys.*, **31**, 100.
[26] Scheidt, W. R., and Reed, C. A., 1981, *Chem. Rev.*, **81**, 543.
[27] Shaik, S., Filatov, M., Schröder, D., and Schwartz, H., 1998, *Chem. Eur. J.*, **4**, 193.
[28] Náray-Szabó, G., 1997, *J. Biol. Inorg. Chem.*, **2**, 135.
[29] Marcus, R. A., and Sutin, N., 1985, *Biochim. Biophys. Acta*, **811**, 265.
[30] Goodin, D. B. and McRee, D. E., 1993 Biochemistry, 32, 765-766.
[31] Choudhury, K., Sundaramoorthy, M., Hickman, A., Yonetani, T. Woehl, E., Dunn, M. F., and Poulos, T. F., 1994, J. Biol. Chem., 269, 20239-20249.
[32] Poulos, T. L., 1996, *J. Biol. Inorg. Chem.*, **1**, 356.
[33] Franzen, S., 2001, *J. Am. Chem. Soc.*, **123**, 12578.
[34] Menyhárd, D. K., and Náray-Szabó, G., 1999, *J. Phys. Chem. B*, **103**, 227.
[35] Wirstam, M., Blomberg, M. R. A., and Siegbahn, P. E. M., 1999, *J. Am. Chem. Soc.*, **121**, 10178.
[36] Green, M. T., 2000, *J. Am. Chem. Soc*., **122**, 9495.
[37] Antony, J., Grodzicki, M., and Trautwein, A. X., 1997, *J. Phys. Chem. A*, **101**, 2692.
[38] Kuramochi, H., Noodleman, L., and Case, D. A., 1997, *J. Am. Chem. Soc.*, **119**, 11442.
[39] Becke, A. D., 1988, *Phys. Rev. A*, **38**, 3098.
[40] Becke, A. D., 1992, *J. Chem. Phys.*, **96**, 2155.
[41] Becke, A. D., 1993, *J. Chem. Phys.*, **98**, 1372.
[42] Becke, A. D., 1993, *J. Chem. Phys.*, **98**, 5648.
[43] Lee, C., Yang, W., and Parr, R. G., 1988, *Phys. Rev. B*, **37**, 785.
[44] Hertwig, R. H., and Koch, W., 1997, *Chem. Phys. Lett.*, **268**, 345.
[45] Bauschlicher, C. W., 1995, *Chem. Phys. Lett.*, **246**, 40.
[46] Jensen, F, 1999, *Introduction to computational chemistry*, John Wiley & Sons.
[47] Siegbahn, P. E. M., and Blomberg, M. R. A., 1999, *Annu. Rev. Phys. Chem.*, **50**, 221.
[48] Alrichs, R., Bär, M., Häser, M., Horn, H., and Kölmel, C., 1989, *Chem. Phys. Lett.*, **162**, 165.
[49] Sigfridsson, E. and Ryde, U., 2001, *J. Phys. Chem. B*, **105**, 5546-5552.
[50] M. H. M. Olsson and U. Ryde, J. Am. Chem. Soc., 123 (2001) 7866-7876.
[51] Schäfer, A., Horn, H., and Ahlrichs, R., 1992, *J. Chem. Phys.*, **97**, 2571.
[52] Exponents: 0.141308 and 0.043402 (*p*); 0.1357 (*d*); and 1.6200 (*f*).
[53] Klamt, A., and Schüürmann, J., 1993, *J. Chem. Soc. Perkin Trans.*, **2**, 799.
[54] Sharp, K. A., 1990, *Annu. Rev. Biophys. Biophys. Chem.*, **19**, 301.
[55] Honig, B., 1995, *Science*, **268**, 1144.
[56] Reiss, H., and Heller, A., 1985, *J. Phys. Chem.*, **89**, 4207.
[57] Sigfridsson, E., and Ryde, U., 2003, *J. Biol. Inorg. Chem.*, **8**, 273.

[58] Seno, Y., Kameda, N., and Otsuka, J., 1980, *J. Chem. Phys.,* **72**, 6048.
[59] Daniel Edwards, W., Weiner, B., and Zerner, M. C., 1986, *J. Am. Chem. Soc.,* **108**, 2196.
[60] Kozlowski, P. M., Spiro, T. G., and Zgierski, M. Z., 2000, *J. Phys. Chem. B,* **104**, 10659.
[61] Rovira, C., Kunc, K., Hutter, J., and Parrinello, M., 2001, *Inorg. Chem.,* **40**, 11.
[62] Schuller, D. J., Wilks, A., Ortiz de Montellano, P. R., and Poulos, T. L., 1999, *Nat. Struct. Biol.*, **6**, 860.
[63] Harris, D. L., and Loew, G. H., 2001, *J. Porphyrins Phthalocyanines*, **5**, 334.
[64] Prabhu, N. V., Dalosto, S. D., Sharp, K. A., Wright, W. W., and Vanderkooi, J. M., 2002, *J. Phys. Chem. B*, **106**, 5561.
[65] Ryde, U, 1999, *Biophys. J.*, **77**, 2777.
[66] Feis, A., Howes, B. D., Indiani, C., and Smulevich, G., 1998, *J. Raman Spectr.*, **29**, 933.
[67] Howes, B. D., Schiødt, C. B., Welinder, K. G., Marzocchi, M. P., Ma, J.-G., Zhang, J., Shelnutt, J. A., and Smulevich, G., 1999, *Biophys. J.*, **77**, 478.
[68] Ryde, U., and Olsson, M. H. M., 2001, *Int. J. Quant. Chem.*, **81**, 335.
[69] Sigfridsson, E., Olsson, M. H. M., and Ryde, U., 2001, *Inorg. Chem.*, **40**, 2509.
[70] Gajhede, M. 2001. In *Handbook of Metalloproteins*, edited by A. Messerschmidt, R. Huber, T. Poulos, and K. Wieghart (Chichester: J. Wiley & Sons), p. 195.
[71] De Santis, L., Carloni, P., 1999, *Proteins: Structure, Function, and Genetics*, **37**, 611.

Table 1. Optimised geometric parameters (Å) of the studied models. The most stable HS states of **4** and **5** have been underlined.

Structure	m	H-Bond	Fe–N_{Im}	Fe–N_{eq}	N–H	O–H	Fe oop
1-Fe^{III}	6	-	2.107	2.068	1.012	-	0.387
1-Fe^{III}	4	-	2.153	2.001	1.010	-	0.226
1-Fe^{III}	2	-	1.947	1.997	1.011	-	0.223
1-Fe^{II}	5	-	2.214	2.091	1.010	-	0.281
1-Fe^{II}	3	-	2.336	2.018	1.012	-	0.125
1-Fe^{II}	1	-	1.956	2.014	1.009	-	0.223
2-Fe^{III}	6	-	1.966	2.097	-	-	0.498
2-Fe^{III}	4	-	2.007	2.019	-	-	0.298
2-Fe^{III}	2	-	1.857	2.004	-	-	0.235
2-Fe^{II}	5	-	2.057	2.155	-	-	0.625
2-Fe^{II}	3	-	2.118	2.032	-	-	0.252
2-Fe^{II}	1	-	1.948	2.014	-	-	0.175
3-Fe^{III}	6	NH–O	2.090	2.070	1.022	1.931	0.400
3-Fe^{III}	4	NH–O	2.137	2.003	1.020	1.951	0.235
3-Fe^{III}	2	NH–O	1.978	1.999	1.021	1.941	0.223
3-Fe^{II}	5	NH–O	2.208	2.093	1.015	2.077	0.292
3-Fe^{II}	3	NH–O	2.320	2.018	1.013	2.092	0.132
3-Fe^{II}	1	NH–O	1.956	2.014	1.010	2.072	0.153
4-Fe^{III}	6	N–HO	1.979	2.093	1.709	1.017	0.487
4-Fe^{III}	4	N–HO	2.025	2.018	1.680	1.023	0.296
4-Fe^{III}	2	N–HO	1.865	2.002	1.706	1.017	0.234
4-Fe^{II}	5	N–HO	2.080	2.145	1.502	1.080	0.590
4-Fe^{II}	5	NH–O	2.112	2.133	0.999	1.672	0.541
4-Fe^{II}	3	NH–O	2.210	2.026	1.089	1.543	0.197
4-Fe^{II}	1	N–HO	1.953	2.014	1.425	1.116	0.170
5-Fe^{III}	6	N–HO	1.990	2.090	1.825	0.997	0.476
5-Fe^{III}	6	NH–O	2.026	2.082	1.001	1.604	0.451
5-Fe^{III}	4	N–HO	2.036	2.016	1.784	1.000	0.288
5-Fe^{III}	2	N–HO	1.872	2.002	1.816	0.998	0.232
5-Fe^{II}	5	NH–O	2.138	2.109	1.089	1.523	0.403
5-Fe^{II}	5	N–HO	2.084	2.143	1.667	0.997	0.584
5-Fe^{II}	3	NH–O	2.251	2.023	1.080	1.566	0.175
5-Fe^{II}	1	NH–O	1.956	2.014	1.090	1.531	0.162

Table 2. Energy differences (kJ/mole) of optimised high-spin hydrogen bond minima.

	Lowest minima	= 1	= 4	= 80
4-Fe^{III}	N–OH[a]	37.3	15.9	4.0
4-Fe^{II}	NH–O	1.4	8.1	10.5
5-Fe^{III}	N–HO	10.0	9.8	7.0
5-Fe^{II}	N–HO	0.9	1.5	3.4

[a]No minimum was obtained for the NH–H form in vacuum and at = 4. The values in the table were obtained by constraining the N–H bond length to 1.111 Å.

Table 3. Relative energies (kJ/mole) of optimised ground states in vacuum and with = 80. Figures in bold face signifies hydrogen bonds of the NH–O type; others are of the N–HO.

= 1	**1**-Fe^{III}	**2**-Fe^{III}	**3**-Fe^{III}	**4**-Fe^{III}	**5**-Fe^{III}	**1**-Fe^{II}	**2**-Fe^{II}	**3**-Fe^{II}	**4**-Fe^{II}	**5**-Fe^{II}
HS	**24**	0	**21**	0	3	**4**	0	**3**	**0**/1	0/**1**
IS	**0**	7	**0**	3	0	**0**	33	**0**	**17**	**17**
LS	**42**	12	**48**	13	15	**28**	46	**27**	42	**35**

= 80	**1**-Fe^{III}	**2**-Fe^{III}	**3**-Fe^{III}	**4**-Fe^{III}	**5**-Fe^{III}	**1**-Fe^{II}	**2**-Fe^{II}	**3**-Fe^{II}	**4**-Fe^{II}	**5**-Fe^{II}
HS	**20**	3	**19**	6	10	**1**	0	**0**	**0**/12	0/**3**
IS	**0**	0	**0**	0	0	**0**	23	**0**	**10**	**16**
LS	**36**	17	**45**	20	23	**26**	43	**26**	52	**41**

Table 4. Atomic charges and spin densities for the investigated systems.

No.	Spin	H-bond	Charge on			Spin density on		
		type	Fe	N_{Im}	N_{eq}	Fe	N_{eq}	N_{im}
1	6	-	1.01	–0.51	–0.63	4.19	0.51	0.09
	4	-	0.89	–0.46	–0.60	2.83	–0.08	0.10
	2	-	0.82	–0.46	–0.58	1.16	–0.18	–0.06
	5	-	0.83	–0.43	–0.61	3.81	0.16	0.04
	3	-	0.71	–0.39	–0.58	2.07	–0.10	0.04
	1	-	0.65	–0.40	–0.55	-	-	-
2	6	-	0.99	–0.56	–0.61	4.16	0.45	0.20
	4	-	0.87	–0.51	–0.59	2.71	–0.08	0.20
	2	-	0.79	–0.47	–0.57	1.02	–0.09	–0.01
	5	-	0.73	–0.53	–0.56	3.73	0.13	0.04
	3	-	0.70	–0.45	–0.57	2.07	–0.05	0.08
	1	-	0.63	–0.40	–0.55	-	-	-
3	6	NH–O	1.00	–0.52	–0.62	4.19	0.51	0.09
	4	NH–O	0.88	–0.47	–0.60	2.83	–0.08	0.10
	2	NH–O	0.81	–0.46	–0.58	1.18	–0.05	–0.05
	5	NH–O	0.82	–0.43	–0.60	3.81	0.16	0.04
	3	NH–O	0.71	–0.40	–0.58	2.07	–0.10	0.04
	1	NH–O	0.65	–0.41	–0.55	-	-	-
4	6	<u>N–HO</u>	1.01	–0.58	–0.62	4.18	0.45	0.18
	4	N–HO	0.87	–0.51	–0.59	2.74	–0.08	0.18
	2	N–HO	0.79	–0.47	–0.57	1.04	–0.09	–0.02
	5	N–HO	0.74	–0.53	–0.56	3.73	0.13	0.04
		<u>NH–O</u>	0.76	–0.52	–0.57	3.74	0.12	0.05
	3	NH–O	0.71	–0.44	–0.58	2.06	–0.08	0.05
	1	N–HO	0.64	–0.41	–0.55	-	-	-
5	6	<u>N–HO</u>	1.00	–0.56	–0.62	4.18	0.46	0.16
		NH–O	1.01	–0.55	–0.63	4.19	0.48	0.18
	4	N–HO	0.87	–0.51	–0.59	2.76	–0.09	0.17
	2	N–HO	0.80	–0.47	–0.57	1.05	–0.10	–0.02
	5	NH–O	0.82	–0.48	–0.60	3.81	0.17	0.04
		<u>N–HO</u>	0.75	–0.53	–0.57	3.73	0.13	0.05
	3	NH–O	0.71	–0.43	–0.58	2.07	–0.09	0.05
	1	NH–O	0.65	–0.42	-0.55	-	-	-

Table 5. Reorganisation energies (kJ/mole) of the investigated models.

No.	Spin state	Full model			No acetate and backbone			Fe^{III} form	Fe^{II} form
		red	ox		red	ox			
1	HS	14	15	28	-	-	-	-	-
	IS	13	61	74	-	-	-	-	-
2	HS	40	21	61	-	-	-	-	-
	IS	24	61	85	-	-	-	-	-
3	HS	54	42	96	15	13	29	-	-
	IS	33	64	97	-	-	-	-	-
4	HS	28	26	54	22	11	33	N–HO	N–HO
	IS	30	49	79	22	45	66	N–HO	NH–O
5	HS	31	30	61	26	4	30	N–HO	NH–O
	IS	35	28	63	25	4	29	N–HO	NH–O

Table 6. Reduction potentials (V) of the investigated models, calculated at various values of the dielectric constant.

No.	Spin	Fe^{III} form	Fe^{II} form	= 1	= 4	= 80
1	HS	-	-	0.86	0.03	–0.34
	IS	-	-	0.66	–0.17	–0.54
	LS	-	-	0.8	–0.06	–0.44
2	HS	-	-	–2.31	–1.21	–0.66
	IS	-	-	–2.58	–1.48	–0.93
	LS	-	-	–2.65	–1.53	–0.97
3	HS	NH–O	NH–O	0.72	–0.03	–0.37
	IS	NH–O	NH–O	0.53	–0.23	–0.56
	LS	NH–O	NH–O	0.75	–0.02	–0.36
4	HS	N–HO	N–HO	–2.00	–0.98	–0.47
		N–HO	N–HO	–2.01	–1.06	–0.58
	IS	N–HO	NH–O	–2.14	–1.12	–0.62
	LS	N–HO	N–HO	–2.30	–1.33	–0.84
5	HS	N–HO	N–HO	–1.75	–0.86	–0.44
		N–HO	NH–O	–1.74	–0.84	–0.39
		NH–O	N–HO	–1.86	–0.96	–0.50
		NH–O	NH–O	–1.85	–0.94	–0.46
	IS	N–HO	NH–O	–1.93	–1.07	–0.64
	LS	N–HO	NH–O	–1.96	–1.09	–0.65

Figure 1. The models investigated in this study: optimised structures for HS Fe^{III} porphine with a neutral imidazole ligand (**1**), a negatively charged imidazolate ligand (**2**), an imidazole ligand with an internal hydrogen bond to a carbonyl group (**3**), an imidazole ligand, hydrogen bonded to an acetate group (**4**), or an imidazole ligand with both the carbonyl and acetate groups (**5**).

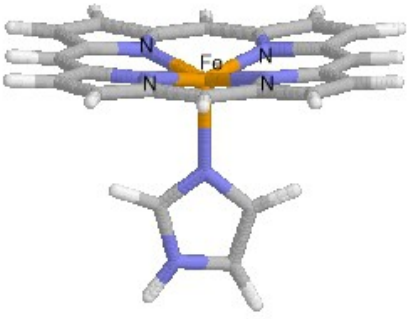

1

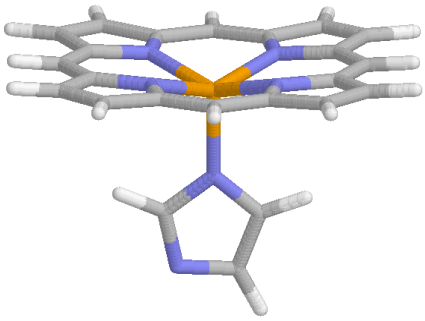

2

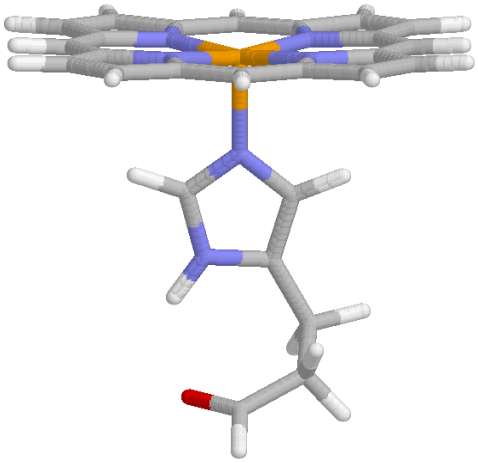

3

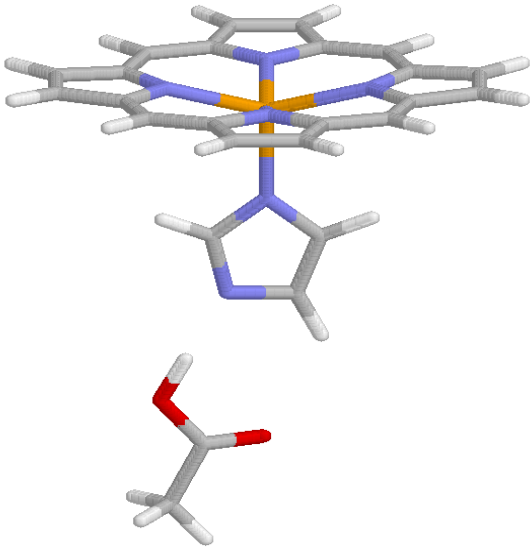

4

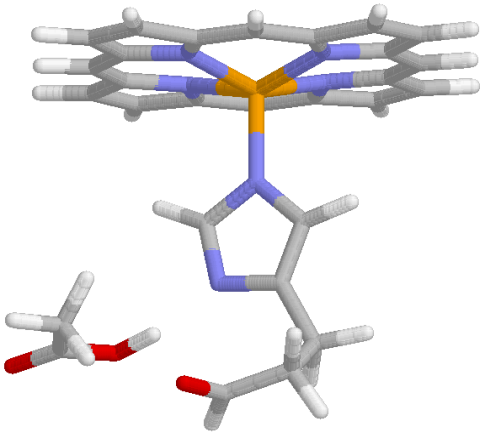

5

Figure 2. Relaxed energy profiles for the hydrogen bond of the HS ferrous model **4**, calculated at various values of the dielectric constant.

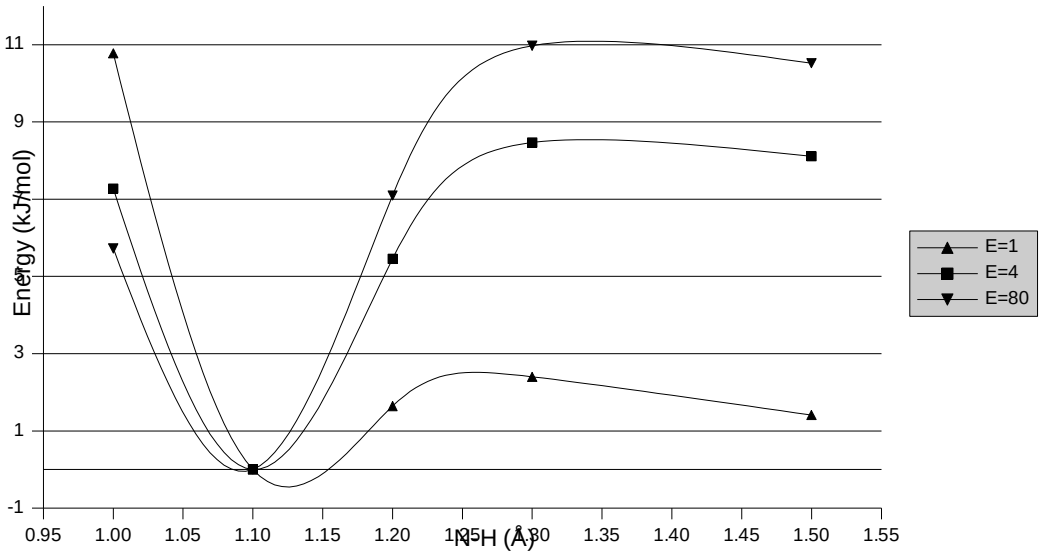

Figure 3. Influence of the imidazole N–H bond length on various properties for the HS model **4**; a) iron Mulliken charge, b) Fe–N_{Im} bond distance, and c) the distance of the iron ion out of the porphyrin plane.

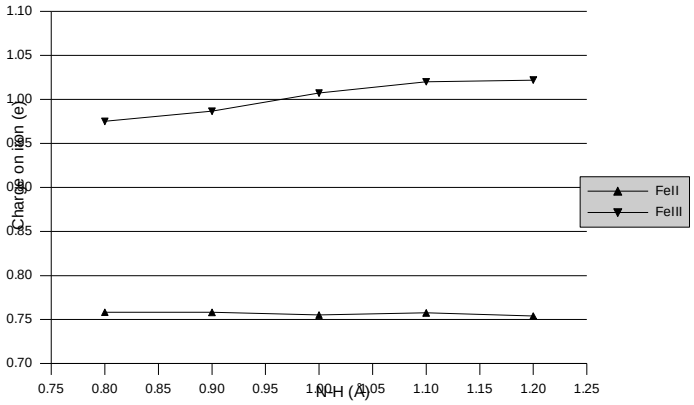

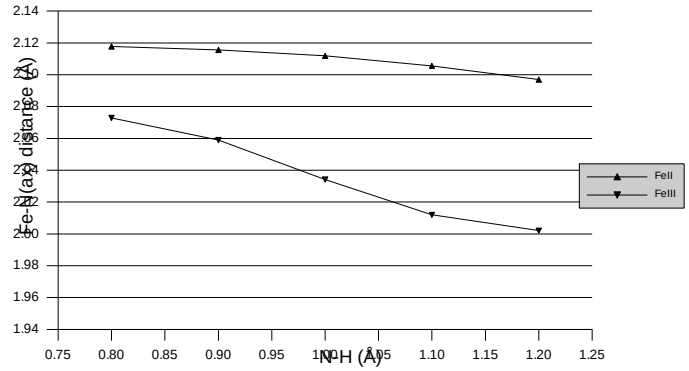

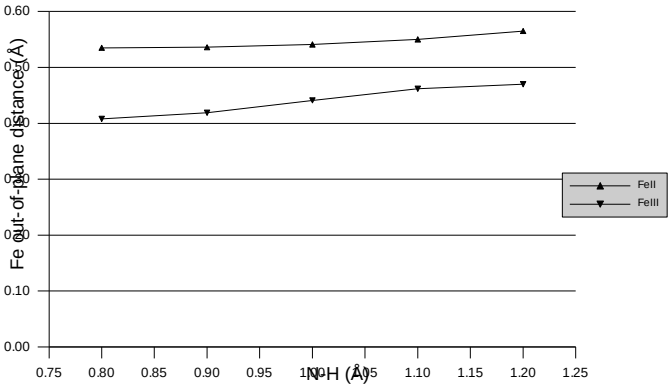

Figure 4. Relaxed energy profiles of the two hydrogen bonds of HS ferric model **5**, calculated at various values of the dielectric constant.

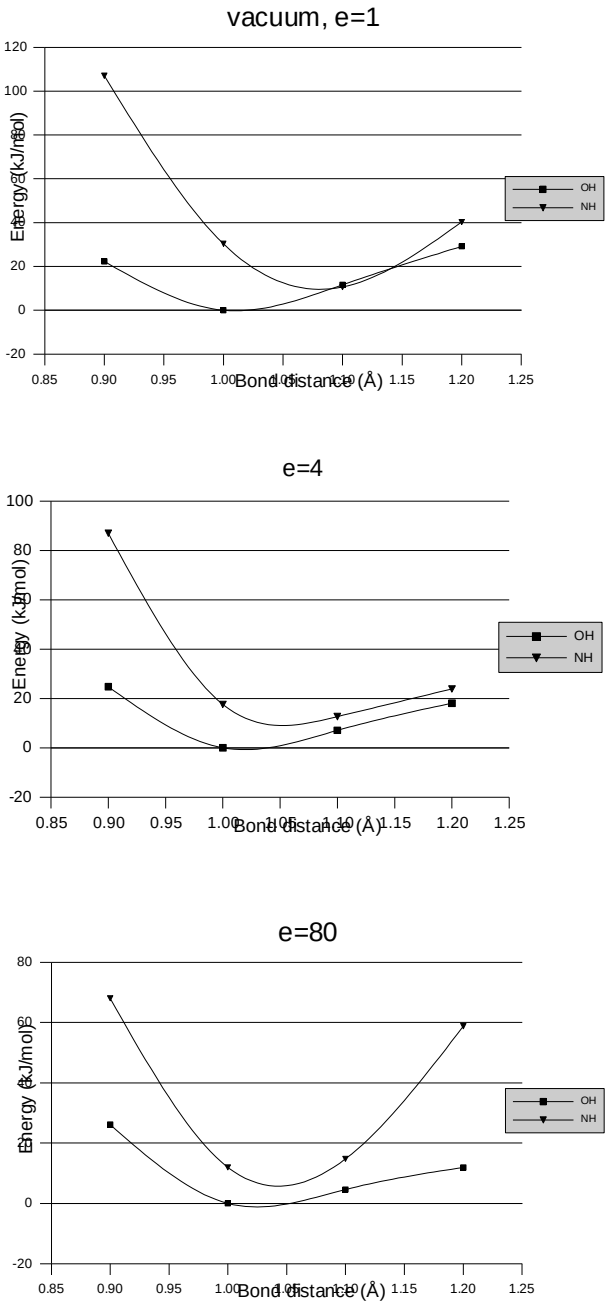

Figure 5. Relaxed energy profiles of the two hydrogen bonds of HS ferrous model **5**, calculated at various values of the dielectric constant.

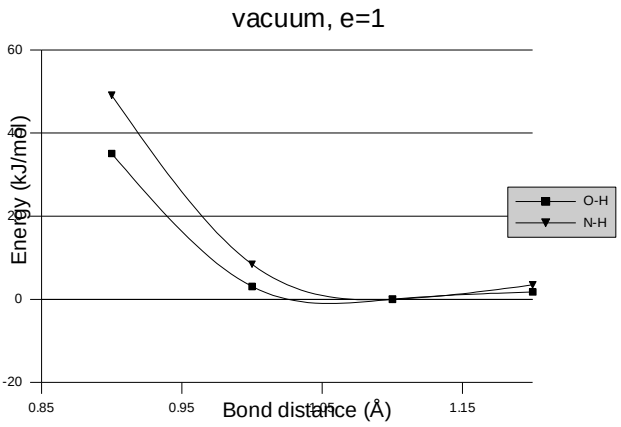
vacuum, e=1
60
40
20
0
-20
Energy (kJ/mol)
0.85
0.95
1.05
1.15
Bond distance (Å)
O-H
N-H

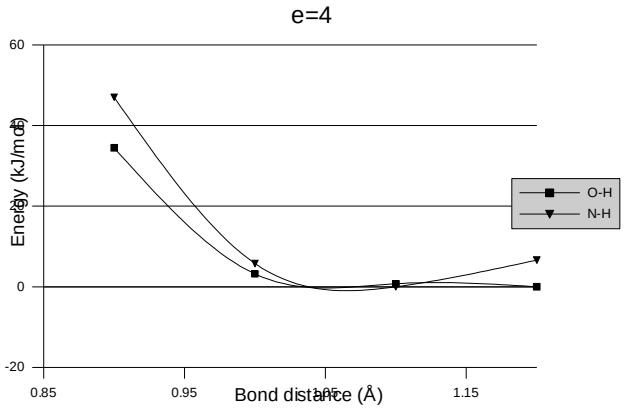
e=4
60
40
20
0
-20
Energy (kJ/mol)
0.85
0.95
1.05
1.15
Bond distance (Å)
O-H
N-H

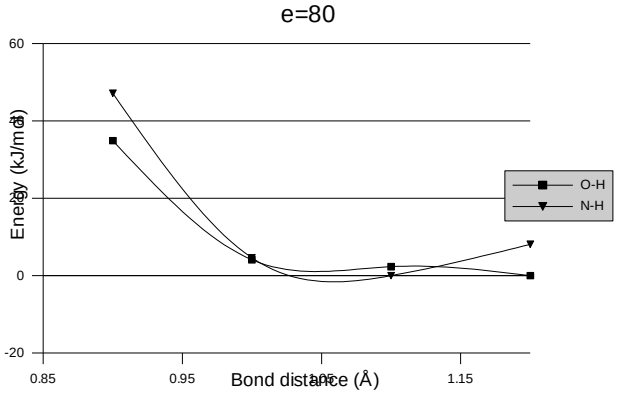
e=80
60
40
20
0
-20
Energy (kJ/mol)
0.85
0.95
1.05
1.15
Bond distance (Å)
O-H
N-H